Modelling Study on the Plasma Flow and Heat Transfer in a Laminar Arc Plasma Torch Operating at Atmospheric and Reduced Pressure*

WANG Haixing (王海兴)[1], CHEN Xi (陈熙)[2], PAN Wenxia (潘文霞)[3]

[1]School of Astronautics, Beijing University of Aeronautics and Astronautics, Beijing 100191, China
[2]Department of Engineering Mechanics, Tsinghua University, Beijing 100084, China
[3]Institute of Mechanics, Chinese Academy of Sciences, Beijing 100190, China

Abstract A modelling study is performed to investigate the characteristics of both plasma flow and heat transfer of a laminar non-transferred arc argon plasma torch operated at atmospheric and reduced pressure. It is found that the calculated flow fields and temperature distributions are quite similar for both cases at a chamber pressure of 1.0 atm and 0.1 atm. A fully developed flow regime could be achieved in the arc constrictor-tube between the cathode and the anode of the plasma torch at 1.0 atm for all the flow rates covered in this study. However the flow field could not reach the fully developed regime at 0.1 atm with a higher flow rate. The arc-root is always attached to the torch anode surface near the upstream end of the anode, i.e. the abruptly expanded part of the torch channel, which is in consistence with experimental observation. The surrounding gas would be entrained from the torch exit into the torch interior due to a comparatively large inner diameter of the anode channel compared to that of the arc constrictor-tube.

Keywords: non-transferred arc torch, plasma flow and heat transfer, numerical modelling

PACS: *52.80.Mg, 52.65.Kj, 47.27.Te*

1 Introduction

DC non-transferred arc plasma torches have been used to generate thermal plasmas in various industrial applications, such as atmospheric or sub-atmospheric plasma spraying, thermal plasma waste treatment, plasma-assisted chemical vapour deposition, and plasma preparation of ultra-fine powders [1~6]. Although there have been a lot of experimental and modelling results concerning the thermal plasma characteristics in the literature [1~20], the understanding about DC non-transferred arc plasma characteristics is still insufficient. The physical processes in a non-transferred arc plasma torch are quite complicated. The plasma flow and heat transfer are coupled with the electromagnetic field. There always exists a large temperature difference in the thermal plasma system and thus temperature-dependent thermodynamic and transport properties of the plasma must be considered in any theoretical study. Many other complicated factors are also often involved such as the unsteady effects caused by arc-root fluctuation, the non-local thermodynamic equilibrium (non-LTE) effects near the electrodes or cold walls, etc.

Most published modelling studies on the DC non-transferred arc plasma torches are concerned with the case working at atmospheric pressure, e.g. in Ref. [7~18] and the references cited therein. However, thermal plasmas generated at sub-atmospheric pressure are of special interest for many material processing applications, such as the preparation of large-area diamond films or other functional films with higher deposition rates [3,5]. The reason is that rather high densities of active particles are involved in the thermal plasma generated at sub-atmospheric pressure in comparison with low-pressure discharge plasmas, or cold plasmas. Recently, a DC non-transferred arc plasma torch operated at sub-atmospheric pressure has been established at the Institute of Mechanics of the Chinese Academy of Sciences, and a series of experimental results have been obtained [19,20]. These results are about the plasma torch characteristics at different parameters, including the vacuum -chamber pressure ($10^2 \sim 10^5$ Pa), arc current (80~130 A), types of working gas (Ar, Ar-H_2, Ar-N_2, etc.) and different gas flow-rates associated with laminar and turbulent flow regimes. The effects of an applied magnetic field of 100 Gauss to 450 Gauss on the plasma torch characteristics have also been examined. Especially, the arc-root attachment modes have been successfully observed using a specially designed copper reflection mirror in coordination with an ICCD (intensified charge coupled device) camera. The copper mirror carries a thin boron-nitride film about 20 mm in diameter at its center and thus can reduce the interference of the intensive light emitted from the high-temperature arc column upon the observation of the weakly luminous arc-root on the anode surface. When pure argon is used as the plasma-forming gas, it is found that the

* supported by National Natural Science Foundation of China (Nos. 10575127, 10772016) and the Doctoral Research Fund of Higher Education of China (No. 20070006022)

arc-root attachment mode is diffusive and circumferentially uniformly distributed at the anode surface and that the plasma jet issued from the plasma torch is stable and axi-symmetrical in the case of a laminar flow regime (at lower flow rates) and without an applied magnetic field [19,20].

Our modelling study is conducted to understand the features of the DC non-transferred arc plasma torch as schematically shown in Fig. 1, which is almost the same as that used in the experimental investigations [19,20]. Preliminary modelling results are presented in this paper to compare the characteristics of plasma flow and heat transfer of the plasma torch operated at 0.1 atm and 1 atm.

2 Modelling approach

The main assumptions employed in this study are as follows. **a.** Both the plasma-forming gas and surrounding gas, in the vacuum chamber outside the plasma torch, are argon. **b.** The flow is steady, laminar and axi-symmetrical. **c.** The plasma is in a local thermodynamic equilibrium (LTE) state and optically thin to radiation. **d.** The flow-induced electrical field ($\mathbf{V}\times\mathbf{B}$) can be ignored in comparison with the static electrical field ($\mathbf{E}$). It is noted that the axi-symmetrical flow assumption is reasonable since the circumferentially uniformly distributed arc-root attachment and the axi-symmetrical laminar plasma jet were observed in the case with argon as the plasma-forming gas [19,20]. In the case without an applied magnetic field, $\mathbf{V}\times\mathbf{B}$ would be small compared with $\mathbf{E}$ since the magnetic field generated by the arc current itself is comparatively small. The LTE assumption is adopted in this preliminary study as the first approximation and will be relaxed in subsequent studies.

Based on the foregoing assumptions, the governing equations in cylindrical coordinates can be written as follows [21].

Mass conservation equation

$$\frac{\partial}{\partial z}(\rho u)+\frac{1}{r}\frac{\partial}{\partial r}(r\rho v)=0. \tag{1}$$

Momentum conservation equations

$$\frac{\partial(\rho uu)}{\partial z}+\frac{1}{r}\frac{\partial(r\rho uv)}{\partial r}=-\frac{\partial p}{\partial z}+2\frac{\partial}{\partial z}\Big(\mu\frac{\partial u}{\partial z}\Big)+\frac{1}{r}\frac{\partial}{\partial r}\Big[r\mu\Big(\frac{\partial u}{\partial r}+\frac{\partial v}{\partial z}\Big)\Big]+j_rB_\theta, \tag{2}$$

$$\frac{\partial(\rho uv)}{\partial z}+\frac{1}{r}\frac{\partial(r\rho vv)}{\partial r}=-\frac{\partial p}{\partial r}+\frac{2}{r}\frac{\partial}{\partial r}\Big(r\mu\frac{\partial v}{\partial r}\Big)+\frac{\partial}{\partial z}\Big[\mu\Big(\frac{\partial v}{\partial z}+\frac{\partial u}{\partial r}\Big)\Big]-2\mu\frac{v}{r^2}+\rho\frac{w^2}{r}-j_zB_\theta, \tag{3}$$

$$\frac{\partial(\rho uwr)}{\partial z}+\frac{1}{r}\frac{\partial(r^2\rho vw)}{\partial r}=\frac{\partial}{\partial z}\Big[\mu\frac{\partial(rw)}{\partial z}\Big]+\frac{1}{r}\frac{\partial}{\partial r}\Big[r\mu\frac{\partial(rw)}{\partial r}\Big]-\frac{2}{r}\frac{\partial(\mu rw)}{\partial r}. \tag{4}$$

Energy conservation equation

$$\frac{\partial(\rho uh)}{\partial z}+\frac{1}{r}\frac{\partial(\rho rvh)}{\partial r}=\frac{\partial}{\partial z}\Big(\frac{\kappa}{C_{\rm p}}\frac{\partial h}{\partial z}\Big)+\frac{1}{r}\frac{\partial}{\partial r}\Big(r\frac{\kappa}{C_{\rm p}}\frac{\partial h}{\partial r}\Big)+u\frac{\partial p}{\partial x}+v\frac{\partial p}{\partial z}+\Phi+\frac{j_z^2+j_r^2}{\sigma}+\frac{5k_{\rm B}}{2e}\Big(\frac{j_z}{C_{\rm p}}\frac{\partial h}{\partial z}+\frac{j_r}{C_{\rm p}}\frac{\partial h}{\partial r}\Big)-U_r. \tag{5}$$

Electrical potential (current continuity) equation

$$\frac{1}{r}\frac{\partial}{\partial r}\Big(r\sigma\frac{\partial\phi}{\partial r}\Big)+\frac{\partial}{\partial z}\Big(\sigma\frac{\partial\phi}{\partial z}\Big)=0. \tag{6}$$

In Eqs. (1)∼(6) u, v and, w are the axial (z-), radial (r-) and circumferential (θ-) velocity components; p, h and ϕ the gas pressure, specific enthalpy and electrical potential; $k_{\rm B}$ and e the Boltzmann constant and elementary charge; whereas ρ, μ, κ, $c_{\rm p}$, σ and U_r are the temperature- and pressure-dependent gas density, viscosity, thermal conductivity, specific heat at constant pressure, electric conductivity and radiation power per unit volume of plasma, respectively, and are calculated in this study by use of a pre-compiled plasma database. Φ in Eq. (5) is the viscous dissipation, and is calculated by

$$\Phi=\mu\Bigg\{2\bigg[\Big(\frac{\partial u}{\partial z}\Big)^2+\Big(\frac{\partial v}{\partial r}\Big)^2+\Big(\frac{v}{r}\Big)^2\bigg]+\Big(\frac{\partial v}{\partial z}+\frac{\partial u}{\partial r}\Big)^2+\Big(\frac{\partial w}{\partial z}\Big)^2+\Big(\frac{\partial w}{\partial r}-\frac{w}{r}\Big)^2\Bigg\}-\frac{2}{3}\mu\Big(\frac{\partial u}{\partial z}+\frac{\partial v}{\partial r}+\frac{v}{r}\Big)^2. \tag{7}$$

Both the pressure work and viscous dissipation terms have been included in the Eq. (5) in order to be applicable to a high velocity flow at a lower gas pressure. The current density components j_r and j_z appearing in Eqs. (2), (3) and (5) are calculated by

$$j_r=-\sigma\frac{\partial\phi}{\partial r},\quad j_z=-\sigma\frac{\partial\phi}{\partial z}, \tag{8}$$

whereas the self-induced magnetic induction intensity B_θ is calculated from

$$B_\theta=\frac{\mu_0}{r}\int_0^r j_z\xi{\rm d}\xi. \tag{9}$$

with μ_0 the magnetic permeability.

The computational domain used in the modelling is denoted as A-B-C-D-E-F-G-H-I-A in Fig. 1, in which A-B-I-A is the cathode, E-F-G-K-E the anode or the wall of the abruptly expanded channel, C-D-E-J-C the insulating inter-electrode insert, referred to as the arc constrictor-tube hereinafter, B-C the inlet of the axially flowing working gas, C-J the inner surface of the arc constrictor-tube, G-H the torch exit, whereas 1 and 2 represent two inlets of the tangentially inflowing working-gas. The boundary conditions required for the numerical simulation are listed in Table 1. Vanishing velocity components and constant temperatures are specified at all solid boundaries; axi-symmetrical conditions are employed along the torch axis; one-way conditions are used at the torch exit; and zero currents

Table 1. Boundary conditions used for solving the governing equations

	u	v	rw	h	ϕ
AB	0	0	0	h_c	$\partial\phi/\partial z = I/(A\sigma_c)$
BC	U_{in}	0	0	h_0	$\partial\phi/\partial z = 0$
CD	0	0	0	h_0	$\partial\phi/\partial z = 0$
DE	0	0	0	h_0	$\partial\phi/\partial r = 0$
EF	0	0	0	h_0	0
FG	0	0	0	$\partial h/\partial z = 0$	$\partial\phi/\partial z = 0$
GH	$\partial u/\partial z = 0$	$\partial v/\partial z = 0$	$\partial(rw)/\partial z = 0$	$\partial h/\partial z = 0$	$\partial\phi/\partial z = 0$
HI	$\partial u/\partial r = 0$	0	0	$\partial h/\partial r = 0$	$\partial\phi/\partial r = 0$
IA	0	0	0	$\partial h/\partial r = 0$	$\partial\phi/\partial r = 0$
Inlet 1	0	0	$(rw)_{in}$	h_0	...
Inlet 2	0	0	$(rw)_{in}$	h_0	...

are assumed at all the boundaries except for the cathode and the anode. The cathode body is included in the computational domain, and at the rear end of the cathode (A-B in Fig. 1), $v_z = 0$, $v_r = 0$, $T = 3000$ K and $\partial\phi/\partial z = I/(A\sigma_c)$ are used, where I, A and σ_c are the arc current, cathode end area and the electric conductivity of the cathode material. $\phi = 0$ is set at the outer surface of the anode (E-F in Fig. 1). The inter-electrode insert and anode wall are also included in the computational domain in order to predict more realistic inner wall temperatures of the anode for the case with local arc-root attachment. Total volumetric flow rates of pure argon, the working gas, are in the range of $4.4 \sim 8.8$ slm (standard liters per minute) in this study. The argon is admitted into the plasma torch in three ways, i.e. axially from the upstream annular slot (B-C in Fig. 1), tangentially from hole 1 (see Fig. 1) around the upstream end of the cathode and also tangentially from hole 2 (see Fig. 1) near the upstream section of the abruptly expanded channel or the anode. The ratios of the flow-rate of axially inflowing gas through inlet A-B to that tangentially inflowing gas through hole 1 and to that tangentially inflowing gas through hole 2 are 1: 1: 1. The inlet velocity at each entry is calculated according to the gas flow rate and corresponding inlet area.

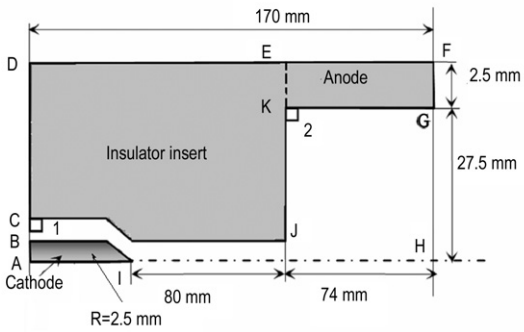

Fig.1 Schematic diagram of the DC non-transferred arc plasma torch under study, the geometric sizes and the computational domain

The SIMPLER algorithm [22] is used to solve the Eqs. (1)∼(6) associated with the auxiliary relations (7)∼(9) and specified boundary conditions listed in Table 1 to obtain the velocity and specific enthalpy (or temperature) distributions in the plasma torch. A mesh of 172 (z-direction)×48 (r-direction) grid points is employed in this study.

3 Results and discussion

Typical modelling results are presented in Figs. 2 ∼6 concerning both the plasma flow and heat transfer characteristics in the DC non-transferred arc plasma torch for the cases with a pressure of 10^5 Pa (or 1.0 atm), an arc current of 80 A to 120 A and an argon flow rate of 4.4 slm to 8.8 slm.

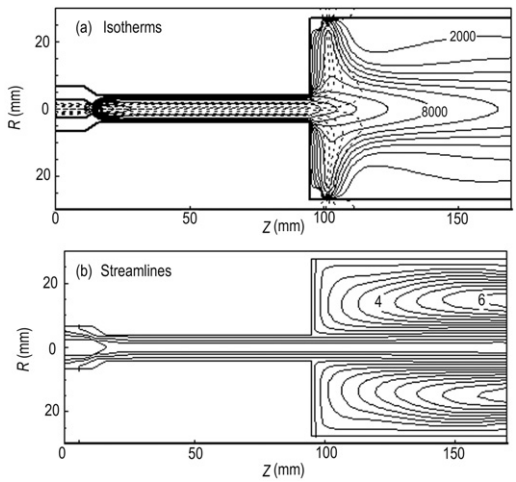

Fig.2 Calculated isotherms (solid lines) (a) and streamlines (b) for the case with an argon flow rate of 4.4 slm, an arc current of 100 A and a gas pressure of 10^5 Pa. Outer isotherm is 2000 K and isotherm interval 1000 K. Streamline interval -0.2×10^{-4} kg·s^{-1} per radian. Electric-current isolines are also shown in (a) as broken lines

Fig. 2 shows the calculated distributions of isotherms (solid lines) as well as electric-current isolines (broken lines) (a) and the streamlines (b) within the non-transferred arc plasma torch for the case with an argon flow rate of 4.4 slm and an arc current of 100 A. Quite similar calculated isolines are also obtained for the flow rates of 6.6 slm and 8.8 slm (not shown as separated figures), but the magnitude of the plasma axial-velocity increases with the increase in gas flow-rate. The predicted isotherms presented in Fig. 2(a) demonstrate that the highest temperature appears at

the location near the cathode tip where the current density assumes its maximum. It is seen from the isotherms and the electric-current isolines shown in Fig. 2(a) that the arc-root in the plasma torch is attached to the anode surface near the upstream end of the anode or the abruptly expanded channel, K-G in Fig. 1. It is found from the calculated streamlines shown in Fig. 2(b) that the surrounding gas outside the plasma torch is entrained from the torch exit into the torch interior due to the fact that the inner diameter of the abruptly expanded channel or the anode is appreciably larger than that of the arc constrictor-tube, C-J in Fig. 1.

Fig. 3 shows the calculated variations in plasma temperature and axial velocity along the torch axis for the cases with a fixed arc current of 100 A and three different flow rates namely 4.4 slm, 6.6 slm and 8.8 slm. It is shown in Fig. 3(a) that the calculated plasma temperatures for all the three different flow rate cases are almost independent of the axial distance within the constrictor tube between the cathode and the anode, i.e. C-J in Fig. 1, with an axial distance less than 95 mm but larger than 70 mm, and the plasma temperature along the torch axis for the axial-distance in a range of 70 mm to 95 mm is maintained at about 12400 K. It means that a fully developed heat transfer regime [23] has been achieved within the arc constrictor-tube for all the three cases with different flow-rates. Fig. 3(b) demonstrates that a fully developed flow regime [23] has also been achieved within the arc constrictor-tube for all the three different flow-rates. Since the arc column is restricted within the constrictor-tube (see Fig. 2),

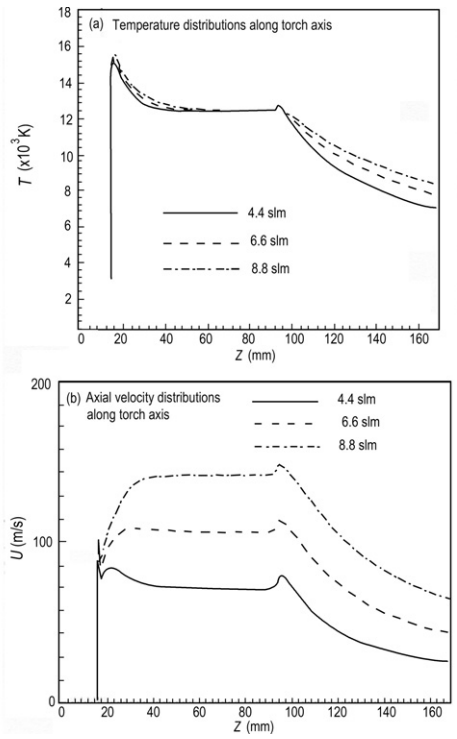

Fig.3 Comparison of calculated variations in the plasma temperature (a) and the axial velocity (b) along the torch axis for three different argon flow rates of 4.4 slm, 6.6 slm and 8.8 slm. Arc current is 100 A and gas pressure is 10^5 Pa

the cold argon inflowing into the constrictor-tube is heated in the constrictor-tube channel and accelerated to a higher velocity. Of course, the magnitude of the axial velocity in the fully developed region increases with the increase in flow rate. The predicted axial velocities in the fully developed plasma flow and heat transfer regime are 70 m/s, 105 m/s and 140 m/s for the cases with the argon flow rates of 4.4 slm, 6.6 slm and 8.8 slm, respectively. This means that the magnitude of the axial velocity near the exit of the arc constrictor-tube axis is directly proportional to the gas flow rate, which is also a typical characteristic of the fully developed flow regime [23]. Fig. 4 shows the calculated variations in plasma temperature (a) and axial velocity (b) along the torch axis for the cases with a fixed flow rate of 4.4 slm and three different arc currents, 80 A, 100 A and 120 A. It is seen from Fig. 4 that the fully developed plasma flow and heat transfer regime can be achieved in the arc constrictor-tube for all the three cases with different arc currents. The predicted plasma temperatures in the fully developed plasma flow and heat transfer regime are 12030 K, 12394 K and 12708 K, and the corresponding axial velocities are 63 m/s, 70 m/s and 78 m/s, respectively, for the arc currents of 80 A, 100 A and 120 A.

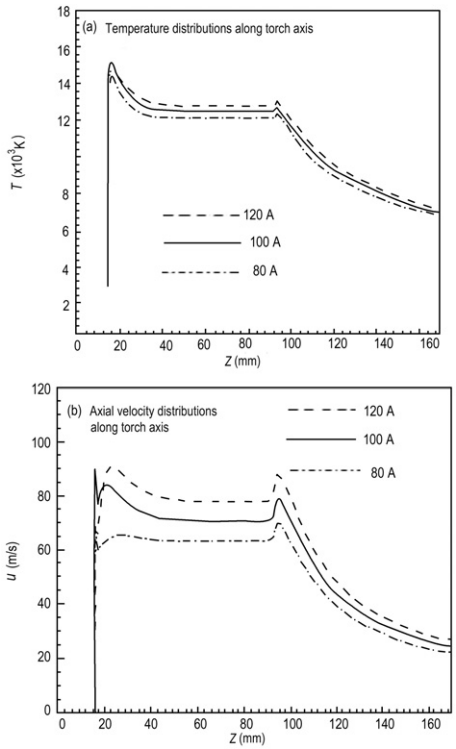

Fig.4 Comparison of calculated variations in the plasma temperature (a) and the axial velocity (b) along the torch axis for three different arc currents, 80 A, 100 A and 120 A. Argon flow rate is 4.4 slm and gas pressure is 10^5 Pa

Fig. 5 compares the calculated radial profiles of the plasma temperatures (a) and axial velocities (b) at the torch exit plane, G-H in Fig. 1, for the cases with a fixed arc current of 100 A and three different flow rates, 4.4 slm, 6.6 slm and 8.8 slm. As is seen in Fig. 5(a)

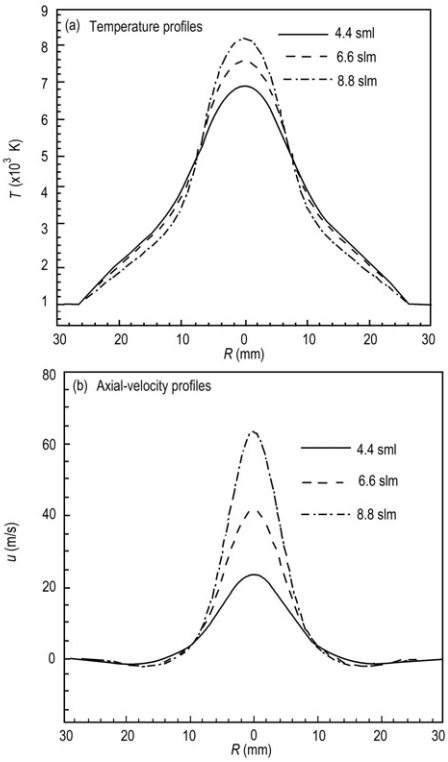

Fig.5 Comparison of calculated radial profiles of the plasma temperature (a) and the axial velocity (b) at the torch exit plane for three different argon flow rates, 4.4 slm, 6.6 slm and 8.8 slm. Arc current is 100 A and gas pressure is 10^5 Pa

and (b), the predicted highest temperatures at the torch exit for the three different flow rates are 6890 K, 7571 K and 8167 K, and the highest axial velocities are 23.6 m/s, 41.9 m/s, 63.5 m/s, respectively. Namely, the highest plasma temperature and axial velocity at the torch exit increase with the increase in the flow rate. Fig. 6 compares the calculated radial profiles of the plasma temperatures (a) and axial velocities (b) at the torch exit plane for the cases with a fixed flow rate of 4.4 slm and three different arc currents 80 A, 100 A and 120 A. Fig. 6(a) and (b) show that the predicted highest temperatures at the torch exit for the three arc currents are 6709 K, 6890 K and 7040 K, and the highest axial velocities are 21.3 m/s, 23.6 m/s and 26.1 m/s, respectively. This means that the highest plasma temperature and axial velocity at the torch exit increase with the increase in arc current. It is noted that negative values of the axial velocity appear at larger radii in Figs. 5(b) and 6(b) due to the existence of a reverse flow from the torch exit to the torch interior.

As the chamber pressure is reduced to 10^4 Pa, or 0.1 atm, the modelling results are presented in Figs. 7∼11 for the plasma flow and heat transfer characteristics in the DC non-transferred arc argon plasma torch. Fig. 7 shows the calculated distributions of isotherms (solid lines) as well as electric-current isolines (brokenlines) (a) and the streamlines (b) within the non-transferred arc plasma torch for the case with an argon flow rate of 4.4 slm and an arc current of 100 A. The calculated isolines obtained for the argon

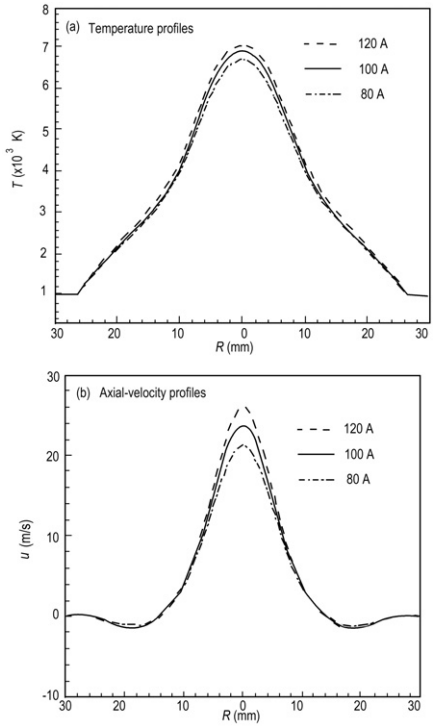

Fig.6 Comparison of calculated radial profiles of the plasma temperature (a) and the axial velocity (b) at the torch exit plane for three different arc currents 80 A, 100 A and 120 A. Argon flow rate is 4.4 slm and gas pressure is 10^5 Pa

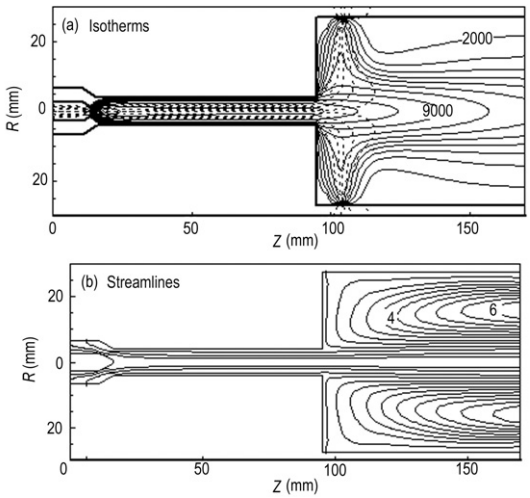

Fig.7 Calculated isotherms (solid lines) (a) and streamlines (b) for the case with an argon flow rate of 4.4 slm, an arc current of 100 A and a gas pressure of 10^4 Pa. Outer isotherm is 2000 K and isotherm interval 1000 K. Streamline interval -0.2×10^{-4} kg·s^{-1} per radian. Electric-current isolines are also shown in (a) as broken lines

flow rates that change to 6.6 slm or 8.8 slm (not shown as separated figures) are quite similar to those shown in Fig. 7, but the magnitudes of the plasma axial-velocity increase with the increase in the flow rate. It is also seen from the isotherms and the electric-current isolines shown in Fig. 7(a) that the arc-root is still attached to the anode surface near the upstream end of the anode surface. Such a result concerning the anode arc-root's location obtained for the chamber pressure

of 10^4 Pa is identical to that presented above for the pressure of 10^5 Pa, and is consistent with experimental observation. It can also be found from the calculated streamlines shown in Fig. 7(b) that the surrounding gas outside the plasma torch is entrained from the torch exit into the torch interior due to the existence of an abruptly expanded part of the torch channel.

Fig. 8 shows the calculated variations of plasma temperature, and axial velocity along the torch axis for a fixed arc current of 100 A and three different flow-rates of 4.4 slm, 6.6 slm and 8.8 slm. The calculated temperature distributions shown in Fig. 8(a) are almost independent of the axial distance within the arc constrictor-tube channel when the axial distance is larger than 80 mm for all the three different flow rates, while the plasma temperature at the torch axis remains at about 12106 K when the axial distance is in the range of 80 mm to 95 mm. This means that a fully developed heat transfer regime is achieved near the exit of the arc constrictor-tube for all the three cases with different flow rates. However, Fig. 8(b) demonstrates that the fully developed flow regime can only be achieved for the case with the argon flow rate of 4.4 slm. The plasma flow does not reach the fully developed regime within the arc constrictor-tube, while the axial velocity increases continuously with the increase in the axial distance, for the cases with argon flow rates of 6.6 slm and 8.8 slm. Fig. 9 shows the calculated variations of plasma temperature and axial velocity along the torch axis for a fixed flow rate of 4.4 slm and three different

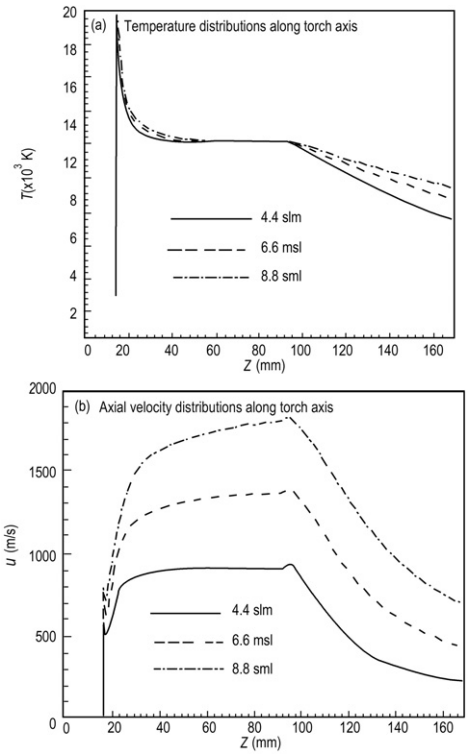

Fig.8 Comparison of calculated variations in the plasma temperature (a) and the axial velocity (b) along the torch axis for three different argon flow rates, 4.4 slm, 6.6 slm and 8.8 slm. Arc current is 100 A and gas pressure is 10^4 Pa

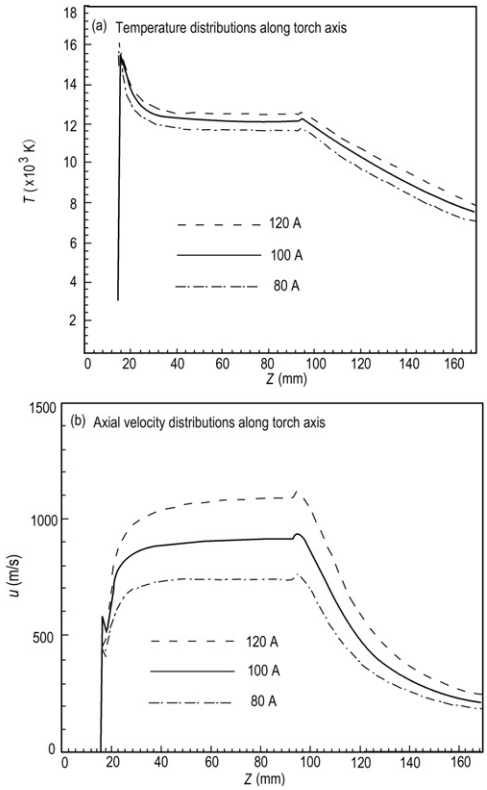

Fig.9 Comparison of calculated variations in the plasma temperature (a) and the axial velocity (b) along the torch axis for three different arc currents 80 A, 100 A and 120 A. Argon flow rate is 4.4 slm and gas pressure is 10^4 Pa

arc currents. Fig. 9(a) and (b) show that, as the argon flow rate is set to be 4.4 slm, the fully developed plasma flow and heat transfer regimes can be achieved in the arc constrictor-tube for all the three cases with different arc currents at 10^4 Pa. In the fully developed regime, the predicted plasma temperatures at the torch axis are 11640 K, 12106 K and 12472 K, and the axial velocities at the torch axis are 742 m/s, 910 m/s and 1087 m/s for the arc currents of 80 A, 100 A and 120 A, respectively. It is noted that for a given flow rate, the predicted highest axial velocities at the axis of the arc constrictor-tube shown in Fig. 8(b) or Fig. 9(b) for the case with a gas pressure of 10^4 Pa are much larger than their counterparts obtained for the case with a gas pressure of 10^5 Pa, shown in Fig. 3(b) or Fig. 4(b), since about 10 times smaller gas mass densities are concerned at 10^4 Pa. As a result, the arc constrictor-tube is not long enough to achieve a fully developed flow regime at higher gas flow rates for 10^4 Pa.

Fig. 10 compares the calculated radial profiles of the plasma temperatures and axial velocities at the torch exit plane, G-H in Fig. 1, for the cases with a fixed arc current at 100 A and three different flow rates at 4.4 slm, 6.6 slm and 8.8 slm. As is shown in Figs. 10(a) and (b), for the three different flow rates, the predicted highest temperatures at the torch exit are 7369 K, 8593 K and 9350 K, and the highest axial-velocities at the torch exit are 213 m/s, 426 m/s and 690 m/s, respectively. This means that the highest plasma temperature and the highest axial velocity at the torch exit

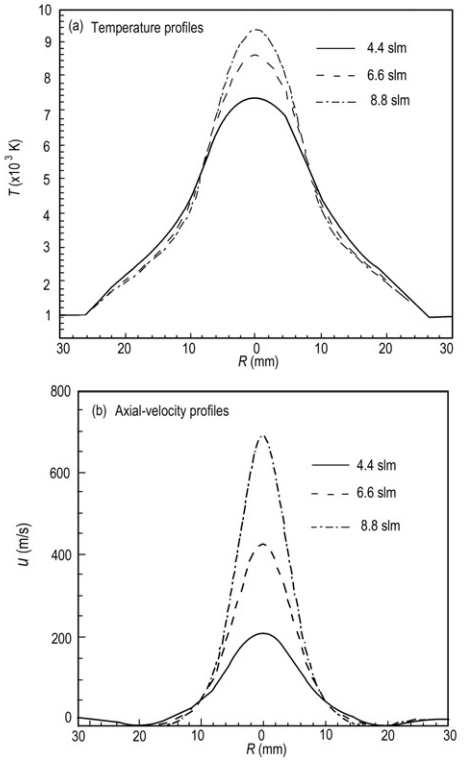

Fig.10 Comparison of calculated radial profiles of the plasma temperature (a) and the axial velocity (b) at the torch exit plane for three different argon flow rates, 4.4 slm, 6.6 slm and 8.8 slm. Arc current is 100 A and gas pressure is 10^4 Pa

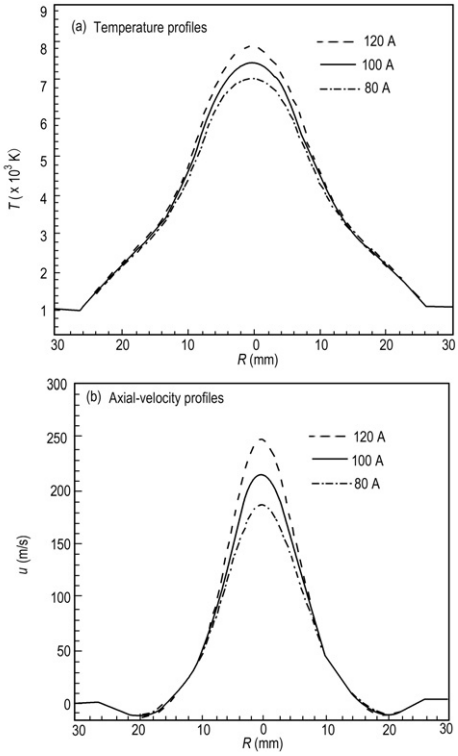

Fig.11 Comparison of calculated radial profiles of the plasma temperature (a) and the axial velocity (b) at the torch exit plane for three different arc currents, 80 A, 100 A and 120 A. Argon flow rate is 4.4 slm and gas pressure is 10^4 Pa

increase with the increase in argon flow rate. Fig. 11 compares the calculated radial profiles of the plasma temperatures and the axial velocities at the torch exit plane for the cases with a fixed flow rate of 4.4 slm and three different arc currents, 80 A, 100 A and 120 A, at a gas pressure of 10^4 Pa. As is shown in Fig. 11(a) and (b), the predicted highest temperatures at the torch exit for the three arc currents are 6960 K, 7369 K and 7820 K, and the corresponding highest axial velocities are 185 m/s, 213 m/s and 246 m/s, respectively. That is, both the highest plasma temperature and the highest axial-velocity at the torch exit increase with the increases in arc currents, similar to the features revealed in the cases at atmospheric pressure. It is noted that negative values of the axial velocity appear at larger radii in Figs. 10(b) and 11(b) due to the existence of a reverse flow from the torch exit to the torch interior. For the case with a fixed volumetric flow rate and arc current, the axial velocities along the torch axis obtained for the gas pressure of 10^4 Pa are much larger than those for the gas pressure of 10^5 Pa since about a 10-fold lower gas density is involved at 10^4 Pa.

Although the predicted location of arc-root attachment, near the upstream end of the anode surface, agrees well with the experimental observation, so far no quantitative experimental data are available to check the predicted plasma temperature and velocity distributions due to the difficulty encountered in the plasma parameter diagnostics within the torch or even in the jet region enclosed by the vacuum chamber. A photograph of the plasma jet outflowing from the plasma torch taken at a chamber pressure of 1.1×10^4 Pa is presented in Fig. 12 to support the present predicted results. Fig. 12 demonstrates that the diameter of the high temperature region of the plasma jet is much less than that of the torch channel exit (G-H in Fig. 1), which is in a qualitative agreement with the modelling predictions shown in Figs. 7(a), 10(a) and 11(a).

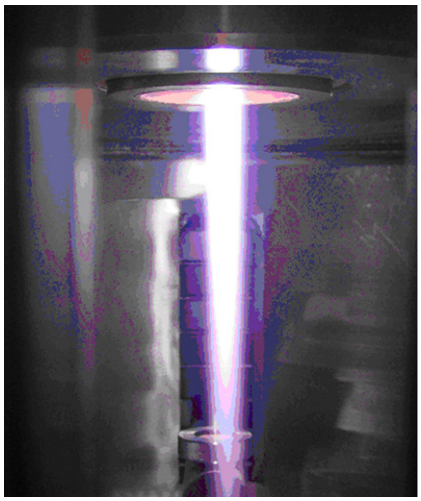

Fig.12 Photograph of the laminar argon plasma jet emitted from the plasma torch with the parameters as arc current of 80 A, argon flow rate of 8.2 slm and chamber pressure of 1.1×10^4 Pa

The SIMPLER algorithm [22] used in this study to solve the governing equations is not applicable to the case where higher Mach numbers and hence a transonic or even supersonic flow are involved [24]. Instead, the all-speed version [24,25] of the SIMPLE algorithm should be employed for the future modelling study at appreciably lower chamber pressures (e.g. 10^3 Pa or 10^2 Pa). This study employs a continuum approach, and no-slip boundary conditions are used for the plasma velocity at the solid boundaries, i.e. the rarefied gas effects [21,26] are ignored. Such a treatment has been found to be satisfactory for the cases of 10^5 Pa and 10^4 Pa. However, as lower chamber pressures, such as 10^3 Pa or even 10^2 Pa, are concerned, the rarefied gas effects may become appreciable and thus the temperature jump and velocity slip conditions [21,26] should be used along the solid-wall surface. In addition, as the first step in our modelling study, a LTE model, widely used in the modelling of DC arc plasma torches, has been adopted here to simplify the modelling efforts at 10^5 Pa and 10^4 Pa. Non-LTE effects may become appreciable at reduced pressure, and a two-temperature or non-equilibrium model may be required. All those complicated factors should be considered in subsequent modelling studies.

4 Conclusions

Modelling results are presented for both the plasma flow and heat transfer characteristics of the laminar DC non-transferred arc plasma torch operated at a gas pressure of 1.0 atm and 0.1 atm. The effects of the main operational parameters, i.e. the argon flow rate and the arc current, on the plasma flow and heat transfer characteristics have been examined. Within the studied range of operational parameters, it is found that a fully developed flow and heat transfer regime can be achieved in the arc constrictor-tube for all the flow rates and arc currents at 1.0 atm, but a fully developed flow regime is not achieved at higher flow rates at 0.1 atm. The arc-root in the plasma torch is always attached to the anode surface at the location near the upstream end of the torch anode. The surrounding gas outside the plasma torch is always entrained from the torch exit into the torch interior due to the sudden size-expansion of the torch channel.

References

1 Pfender E. 1999, Plasma Chem. Plasma Process., 19: 1

2 Fauchais P, Vardelle A. 2000, Plasma Phys. Control. Fusion, 42: B365

3 Lu Fanxiu, Tang Weizhong, Huang Tianbin, et al. 2001, Diamond and Related Materials, 10: 1551

4 Pan Wenxia, Li Gang, Meng Xian, et al. 2005, Pure Appl. Chem., 77: 373

5 Yoshida T. 2006, Pure and Applied Chemistry, 78: 1093

6 Heberlein J, Murphy A. 2008, J. Phys. D: Appl. Phys., 41: 053001

7 Scott D A, Kovitia P, Haddad G N. 1989, J. Appl. Phys., 66: 5232

8 Westhoff R, Szekely J. 1991, J. Appl. Phys., 70: 3455

9 Murphy A B, Kovitia P. 1993, J. Appl. Phys., 73: 4759

10 Bauchire J M, Gonzalez J J, Gleizes A. 1997, Plasma Chem. Plasma Process., 17: 409

11 Li Heping, Chen Xi. 2002, Chinese Physics, 11: 44

12 Li Heping, Pfender E, Chen Xi. 2003, J. Phys. D: Appl. Phys., 36: 1084

13 Hur M, Kim K S, Hong S H. 2003, Plasma Sources Sci. Technol., 12: 255

14 Park J M, Kim K S, Hwang T H, et al. 2004, IEEE Trans. Plasma Sci., 32: 479

15 Mariaux G, Vardelle A. 2005, Int. J. Thermal Sci., 44: 357

16 Trelles J P, Pfender E, Heberlein J V R. 2006, Plasma Chem. Plasma Process., 26: 557

17 Bhuyan P J, Goswami K S. 2007, IEEE Trans. Plasma Sci., 35: 1781

18 Trelles J P, Pfender E, Heberlein J V R. 2007, J. Phys. D: Appl. Phys., 40: 5635

19 Pan Wenxia, Li Teng, Meng Xian, et al. 2005, Chin. Phys. Lett., 22: 2895

20 Pan Wenxia, Meng Xian, Li Teng, et al. 2007, Plasma Science and Technology, 9: 152

21 Chen Xi. 1993, Heat Transfer and Fluid Flow under Thermal Plasma Conditions. Science Press, Beijing (in Chinese)

22 Patankar S V. 1980, Numerical Heat Transfer and Fluid Flow. McGraw-Hill, New York

23 Kays W M, Crawford M E. 1980, Convective Heat and Mass Transfer. 2nd Ed., McGraw-Hill, New York, Chapter 6 & 8

24 Karki K C and Patankar S V. 1989, AIAA Journal, 27: 1167

25 Han Peng, Chen Xi. 2007, Plasma Chem. Plasma Process., 21: 249

26 Lifshitz E M, Pitaevskii L P. 1981, Physical Kinetics. Pergamon, Oxford, p.51∼54

(Manuscript received 7 July 2008)
(Manuscript accepted 6 October 2008)
E-mail address of WANG Haixing: whx@buaa.edu.cn